



HAL
open science

Methyl isocyanate CH₃NCO: An important missing organic in current astrochemical networks

Liton Majumdar, Jean-Christophe Loison, M. Ruaud, P. Gratier, Valentine Wakelam, Audrey Coutens

► **To cite this version:**

Liton Majumdar, Jean-Christophe Loison, M. Ruaud, P. Gratier, Valentine Wakelam, et al.. Methyl isocyanate CH₃NCO: An important missing organic in current astrochemical networks. *Monthly Notices of the Royal Astronomical Society: Letters*, 2017, 473 (1), pp.L59-L63. 10.1093/mnrasl/slx157 . hal-01599691

HAL Id: hal-01599691

<https://hal.science/hal-01599691>

Submitted on 1 Jun 2024

HAL is a multi-disciplinary open access archive for the deposit and dissemination of scientific research documents, whether they are published or not. The documents may come from teaching and research institutions in France or abroad, or from public or private research centers.

L'archive ouverte pluridisciplinaire **HAL**, est destinée au dépôt et à la diffusion de documents scientifiques de niveau recherche, publiés ou non, émanant des établissements d'enseignement et de recherche français ou étrangers, des laboratoires publics ou privés.

Methyl isocyanate CH₃NCO: An important missing organic in current astrochemical networks

L. Majumdar^{1,2*}, J.-C. Loison^{3,4}, M. Ruaud⁵, P. Gratier¹, V. Wakelam¹, A. Coutens¹

¹ *Laboratoire d'astrophysique de Bordeaux, Univ. Bordeaux, CNRS, B18N, allée Geoffroy Saint-Hilaire, 33615 Pessac, France*

² *Jet Propulsion Laboratory, California Institute of Technology, 4800 Oak Grove Drive, Pasadena, CA 91109, USA*

³ *Univ. Bordeaux, ISM, UMR 5255, F-33400 Talence, France*

⁴ *CNRS, ISM, UMR 5255, F-33400 Talence, France*

⁵ *NASA Ames Research Center, Moffett Field, CA 94035, USA*

Accepted XXX. Received YYY; in original form ZZZ

ABSTRACT

Methyl isocyanate (CH₃NCO) is one of the important complex organic molecules detected on the comet 67P/Churyumov-Gerasimenko by *Rosetta's* Philae lander. It was also detected in hot cores around high-mass protostars along with a recent detection in the solar-type protostar IRAS 16293-2422. We propose here a gas-grain chemical model to form CH₃NCO after reviewing various formation pathways with quantum chemical computations. We have used NAUTILUS 3-phase gas-grain chemical model to compare observed abundances in the IRAS 16293-2422. Our chemical model clearly indicates the ice phase origin of CH₃NCO.

Key words: Astrochemistry, ISM: molecules, ISM: abundances, ISM: evolution, methods: statistical

1 INTRODUCTION

Comets are considered to be the repository of the most pristine material from the origin of the solar system in the form of ice, dust, silicate and refractory organic material (Mumma & Charnley 2011). It is believed that some of the water and organic material found on Earth may have been delivered by comets (Hartogh et al. 2011). In the Solar System, when a comet passes close to the Sun, it warms and begin to evaporate their surface and evolve gasses. This process, called outgassing, produces a coma of gas and dust that has been extensively observed (Crovisier 2006). More than 20 organic molecules have been identified in the coma of comets via ground and space-based observations (Biver et al. (2014); Crovisier et al. (2004)). The chemical composition of comets clearly indicates that these objects are populated with many organic compounds that are commonly detected in the ISM. Biver et al. (2015) have found a good correlation between the type of species detected in the coma of comets and those of warm molecular clouds.

Recently, the spacecraft Rosetta has detected many complex organic molecules (COMs) (such as ethanol (CH₃CHO), formamide (NH₂CHO), methyl isocyanate (CH₃NCO), ethylamine (C₂H₅NH₂) and many more) on the material of the comet 67P/Churyumov-Gerasimenko by the COSAC experiment (Goesmann et al. 2015) and even sim-

plest amino acid glycine accompanied by methylamine and ethylamine in the coma measured by the ROSINA (Altwegg et al. 2016). CH₃NCO is one of those organics that could play a role in the synthesis of amino acid chains called peptides (Pascal et al. 2005). It was first detected in Sgr B2 by Halfen et al. (2015) and later in Orion KL by Cernicharo et al. (2016). Recently, it was also detected in the solar-type protostar IRAS 16293-2422 by Martín-Doménech et al. (2017) and Ligterink et al. (2017).

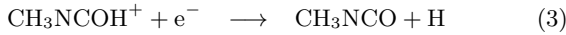
However, it is not well understood how CH₃NCO is formed in the ISM. Recently, Martín-Doménech et al. (2017) has included the chemistry proposed by Halfen et al. (2015) and suggested that the production of CH₃NCO could occur mostly via the gas-phase chemistry after the evaporation of HNCO from grain surface. Belloche et al. (2017) has considered a grain surface production of CH₃NCO in their model via the radical-addition reaction between CH₃ and OCN. Another study by Ligterink et al. (2017) claimed that CH₃NCO can be formed in the solid state by VUV irradiation of CH₄:HNCO mixtures through CH₃ and NCO recombinations. This motivated us to revisit the chemistry of CH₃NCO in the ISM.

This paper reports the first public gas-grain chemical network for CH₃NCO followed by astrochemical modelling of low mass protostar IRAS 16293. The chemistry is presented in Section 2. The chemical model is described in Section 3 while the results are discussed in the last Section.

* E-mail: liton.icsp@gmail.com

2 REVIEW OF THE INTERSTELLAR CHEMISTRY OF CH₃NCO

Despite an intensive search, we did not find any reaction producing efficiently CH₃NCO in the gas phase. Halfen et al. (2015) proposed the following gas phase formation route:



But we have found that reaction 1 is endothermic by 77 kJ/mol and shows a Transition State (TS) located 83 kJ/mol above the entrance level (see Table 4 in the on-line supplementary material) and thus cannot play any role in gas phase neither on grain surface at low temperature. Reaction 2 has been studied experimentally by Wight & Beauchamp (1980) and they observed proton transfer process which forms H₂NCO⁺ and CH₄, instead of CH₃NCOH⁺ and H₂. Reaction 3 has then no impact on the CH₃NCO formation. An alternative could have been the CH₃NC + OH → H + CH₃NCO reaction, which is exothermic by 107 kJ/mol, and may not show any barrier. However, CH₃NC has a low abundance in molecular clouds (Cernicharo et al. (1988); Gratier et al. (2013)). So the reaction CH₃NC + OH → H + CH₃NCO will involve very low fluxes and we can thus neglect this reaction.

The detection of CH₃NCO being limited to warm sources (hot cores and hot corinos) suggests a formation of this molecule on grains rather than in the gas phase (Cernicharo et al. 2016). We have found four potential grain surface reactions which may produce CH₃NCO efficiently. The first one is the s-CH₃ + s-OCN → s-CH₃NCO reaction (here ‘s’ is to represent species on the surface). As it is a reaction between two radicals •CH₃ + •OCN, this reaction is barrierless and leads to CH₃NCO which arises from the pairing up of electrons on the two reactants radicals.

The second one is the CH₃ + OCN⁻ → CH₃NCO + e⁻ reaction which is exothermic by 30 kJ/mol at M06-2X/AVTZ level in the gas phase. The M06-2X highly nonlocal functional is developed by Zhao & Truhlar (2008) and is well suited for structures and energetics of the transition states. OCN⁻ is widely observed on interstellar ice (van Broekhuizen et al. 2005) and CH₃ is supposed to be relatively abundant on ice and relatively mobile (Wakelam et al. 2017), then this reaction may play a role in the CH₃NCO formation. However, the adsorption energy of OCN⁻ on ice is large due to dipole-ion interaction, and even if free electron is also strongly bound to ice (Kammrath et al. (2006); de Koning et al. (2016)), this reaction may be endothermic on ice. By comparison, the H + OCN⁻ → HNCO + e⁻ reaction is more exothermic (by 107 kJ/mol in the gas phase) which should prevent OCN⁻ detection on ice if this reaction was also exothermic on ice due to the importance of H reaction on ice. Then free electron should be less bounded on ice than OCN⁻, as a result CH₃ + OCN⁻ → CH₃NCO + e⁻ reaction is likely endothermic on ice and is neglected here.

Another reaction is induced through the HCN...CO van der Waals formation on ice. As introduced in Ruaud et al. (2015), the proximity of HCN and CO in the van der Waals complex favors the reaction between excited H₂CN* (formed through s-HCN + s-H reaction) and CO (see Table 3 in the

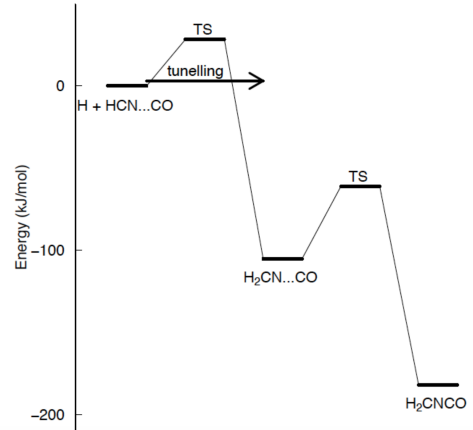


Figure 1. Potential energy diagram for the H + HCN...CO reaction on the doublet surface calculated at the M06-2X/aug-cc-pVTZ level including ZPE.

online supplementary material and Figure 1 for the energy profile diagram of the H + HCN...CO reaction). Then considering the large amount of CO and HCN, this reaction may be important. We then characterise the H + HCN and H₂CN + CO reactions to estimate the importance of these reactions to CH₃NCO formation on ice. The H + HCN → H₂CN shows a notable barrier (computed to be equal to 15.4 kJ/mol (Jiang & Guo 2013), 28.3 kJ/mol at M06-2X/AVTZ level (this work, see Table 2 in the online supplementary material) and 36.4 kJ/mol at CCSD(T)/6-311++G level (Sumathi & Nguyen 1998)). Despite this barrier, this reaction is enhanced on ice due to tunneling (Ruaud et al. 2016), leading to the formation of excited H₂CN*. As the amount of energy in H₂CN* is equal to 105.3 kJ/mol (initially with a very narrow distribution), there is a competition between relaxation and reactivity for all the HCN linked to CO as the transition state for the H₂CN + CO → H₂CNCO is located 44.1 kJ/mol above the H₂CN + CO level, so 61.2 kJ/mol below the energy of the H₂CN* formed through the H + HCN reaction. As the energy distribution of the H₂CN* is initially very narrow, a notable part of the H₂CN* will react with CO. It should be noted that this mechanism of reaction induced through van der Waals complex will also lead to HNCO formation through N...CO + H → HNCO reaction, mechanism which should be very efficient in that case.

The fourth reaction which can produce CH₃NCO is the s-N + s-CH₃CO reaction. The first step, leading to s-CH₃C(N)O in a triplet state, is barrierless characteristic of a radical-radical reaction. The s-CH₃C(N)O can evolve toward s-CH₃ + s-OCN on the triplet surface, isomerize into s-CH₃NCO on the triplet surface or being converted into s-CH₃C(N)O in a singlet state (which can also isomerize into s-CH₃NCO (or s-CH₃OCN) on the singlet surface). Considering the exothermicity of the various step (see Table 6 in the online supplementary material), the formation of s-CH₃NCO is without doubt the most favorable exit channel, either through adduct isomerization or through the recombination of s-CH₃ + s-OCN. Very minor CH₃OCN may also be produced, and some s-CH₃C(N)O may also be stabilized as the TS for dissociation or isomerization are notably

above the CH₃C(N)O energy. s-CH₃C(N)O will react with s-H leading ultimately to CH₃C(O)NH₂ which are however not considered here.

All the introduced and reviewed reactions discussed here are presented in Table 1.

3 ASTROCHEMICAL MODELLING

3.1 The NAUTILUS chemical model

To investigate the chemistry of CH₃NCO in ISM, we have used the state-of-the-art chemical code NAUTILUS described in Ruaud et al. (2016). NAUTILUS computes the chemical composition as a function of time in the gas-phase, and at the surface of dust grains. Here, surface chemistry is solved using the rate equation approximation and assuming a different chemical behaviour between the surface of the mantle and the bulk (i.e. a three-phase model). The equations and the chemical processes included in the model are described in Ruaud et al. (2016). NAUTILUS includes physisorption of gas-phase species on grain surfaces, diffusion of species at the surface of the grains resulting in chemical reactions and several desorption mechanisms. Desorption can be due to the temperature (thermal desorption), cosmic-ray heating (cosmic-ray induced desorption, Hasegawa & Herbst (1993)), UV photon impact (photodesorption) and chemical (Garrod et al. 2007).

3.2 Modification of the network

Our gas phase chemistry is based on the public chemical network kida.uva.2014 (Wakelam et al. 2015a) with the updates on chemistry of HNCO (and their isomers) from the KIDA database¹ and chemistry of CH₃NCO discussed in Section 2 and listed in Table 1 in this work. The surface network is based on the one of Garrod et al. (2007) with several additional processes from Ruaud et al. (2015) and Table 1 in this work. The entire network considered here is available on the KIDA website.

3.3 Physical models

To simulate the chemistry of CH₃NCO in the ISM, we have considered two different physical models which are representative of : (i) dense core and (ii) solar-type protostar (representative of IRAS 16293). For dense core, NAUTILUS is used with homogeneous conditions and integrated over 10⁷ years. The initial elemental abundances are same as in Hincelin et al. (2011) with depleted value of fluorine abundance of 6.68×10⁻⁹ from Neufeld et al. (2005) and we have used a standard C/O ratio of 0.7 (Wakelam et al. (2015b); Majumdar et al. (2016)). The model was run with constant dust and gas temperature of 10 K, a total proton density of 2 × 10⁴ cm⁻³, a cosmic-ray ionization rate of 1.3 × 10⁻¹⁷ s⁻¹, and a visual extinction of 30.

For low mass protostar IRAS 16293, we have used the same physical structure as in Wakelam et al. (2014) and Majumdar et al. (2016) and that was computed using the

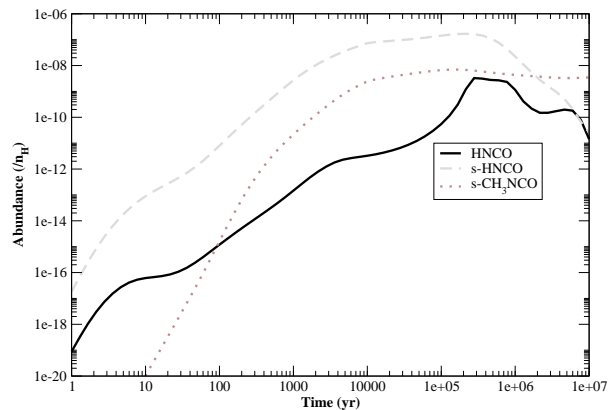


Figure 2. HNCO and CH₃NCO abundances (with respect to H) predicted by our model for typical dense cloud conditions (see section 3.3) as a function of time in the gas-phase and at the surface of the grains (represented by ‘s’). Here, abundance of gas phase CH₃NCO is negligible.

radiation hydrodynamical (RHD) model from Masunaga & Inutsuka (2000). Here the model initially starts from a dense molecular cloud core with a central density $n(\text{H}_2) \sim 3 \times 10^4 \text{ cm}^{-3}$ and the core is extended up to $r = 4 \times 10^4 \text{ AU}$ with a total mass of 3.852 M_\odot . The prestellar core evolves to the protostellar core in $2.5 \times 10^5 \text{ yr}$. When the protostar is formed, the model again follows the evolution for $9.3 \times 10^4 \text{ yr}$, during which the protostar grows by mass accretion from the envelope.

4 RESULTS AND DISCUSSIONS

4.1 Chemistry in dark cloud

Figure 1 shows the time evolution of the abundances of HNCO and CH₃NCO under typical dark cloud conditions. Here, we have shown the chemical evolution of CH₃NCO together with HNCO since in the past HNCO was assumed to be the main precursor for CH₃NCO formation by Martín-Doménech et al. (2017) and Halfen et al. (2015). But this is not the case from our revised chemistry.

Recently, Ruaud et al. (2016) suggested a best fit chemical age for TMC-1 (CP) to be a few 10⁵ years. At this time, 70% of the observed species in TMC-1 (CP) are reproduced by the model within a factor of 10. At 2×10^5 year, abundance of gas phase HNCO predicted by our model is 3×10^{-10} with respect to n_H . This is in good agreement with the observed abundance of 2×10^{-10} in TMC-1 (CP) (Agúndez & Wakelam 2013). At this age, HNCO is formed mainly from the barrier-less surface reaction s-N + s-HCO and the gas phase dissociative recombination reaction of HNCOH⁺.

In our model, CH₃NCO is formed efficiently only in the surface via the reactions of s-H + s-H₂CNCO and

¹ <http://kida.obs.u-bordeaux1.fr/>

Table 1. List of major gas-phase and grain surface reactions added to the model for CH₃NCO formation

Reaction	α	β	γ	Reference
1 HNCO + CH ₃ → CH ₃ NCO + H	1.00×10^{-10}	0	8.04×10^3	[1]
2 CH ₃ NCO + H ₃ ⁺ → CH ₃ NCOH ⁺ + H ₂	1.00×10^{-9}	-0.5	0	[2]
3 CH ₃ NCO + HCO ⁺ → CH ₃ NCOH ⁺ + CO	1.09×10^{-9}	-0.5	0	[2]
4 CH ₃ NCO + H ⁺ → CH ₃ NCO ⁺ + H	1.00×10^{-9}	-0.5	0	[2]
5 CH ₃ NCO + CO ⁺ → CH ₃ NCO ⁺ + CO	1.00×10^{-9}	-0.5	0	[2]
6 CH ₃ NCO + He ⁺ → CH ₃ NCO ⁺ + He	1.00×10^{-9}	-0.5	0	[2]
7 CH ₃ NCO ⁺ + e ⁻ → CH ₃ + OCN	1.50×10^{-7}	-0.5	0	[3]
8 CH ₃ NCOH ⁺ + e ⁻ → CH ₃ NCO + H	3.00×10^{-7}	-0.5	0	[3]
9 CH ₃ NCO + CRP → CH ₃ + OCN	4.00×10^3	0	0	[3]
10 CH ₃ NCO + Photon → CH ₃ + OCN	5.00×10^{-10}	0.0	0	[3]
11 HCN + s-CO → s-HCN...CO	1	0	0	[4]
12 s-HCN...CO + s-H → s-H ₂ CNCO	1	0	2.40×10^3	[5]
13 s-H ₂ CNCO + s-H → s-CH ₃ NCO	1	0	0	[6]
14 s-CH ₃ + s-HNCO → s-CH ₃ NCO	1	0	8.04×10^3	[1]
15 s-CH ₃ + s-OCN → s-CH ₃ NCO	1	0	0	[7]
15 s-CH ₃ + s-OCN ⁻ → s-CH ₃ NCO + e ⁻	0	0	0	[8]
16 s-N + s-CH ₃ CO → s-CH ₃ NCO	1	0	0	[9]

References: [1] Current work and see Table 4 in the online supplementary material for detail calculation [2] [Anicich \(1993\)](#) [3] Considering the similar reactivity of HNCO [4] Following van der Waals formation on ice by [Ruaud et al. \(2015\)](#) [5] Current work and see Table 1 and 2 in the online supplementary material for detail calculation [6] Current work and see Table 3 in the online supplementary material for detail calculation [7] Following [Belloche et al. \(2017\)](#) [8] We neglect this reaction since we don't know exactly the value of the endothermicity. [9] Current work and see Table 6 in the online supplementary material for detail calculation

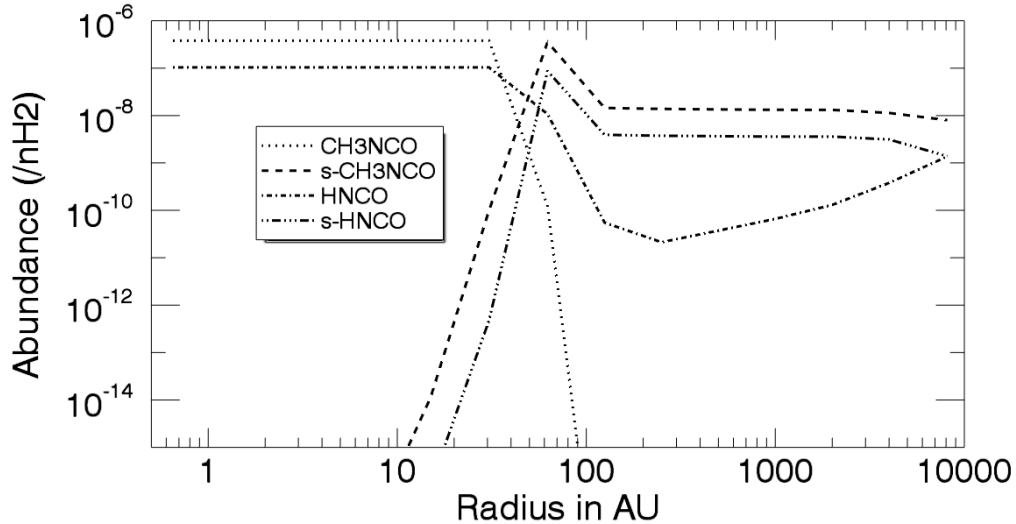


Figure 3. Abundance with respect to H₂ predicted by our low mass protostar model for CH₃NCO and HNCO as a function of distance to the central star. s-CH₃NCO and s-HNCO represent CH₃NCO and HNCO on the grain surface.

s-N + s-CH₃CO since the main gas phase formation route CH₃ + HNCO has an large activation barrier of 8040 K. s-H₂CNCO is formed from the reaction between van der Waals complex s-HCN...CO and highly mobile s-H atoms. Here, s-HCN...CO is considered to be formed when gas phase HCN land on the proximity of s-CO on the grain surfaces ([Ruaud et al. 2015](#)). s-CH₃CO forms mainly via the reaction s-H + s-H₂CCO. The peak gas phase abundance of CH₃NCO from our model is of the order of $\sim 10^{-32}$ with respect to n_H whereas ice phase abundance is 7×10^{-10} around few 10^5 years. This shows that CH₃NCO is frozen in the ices around TMC-1 (CP) (also have lower rotational dipole moment compared to HNCO) and thus not free to rotate. Hence, CH₃NCO is not detectable via its millimeter

wavelength rotational spectra around TMC-1 (CP).

4.2 Chemistry in low mass protostar

In order to validate our chemistry, we present the computed abundances of CH₃NCO, in the gas phase and at the surface of the grains in the protostellar envelope as a function of radius to the central protostar and compare with the observation of CH₃NCO in IRAS 16293. The abundance profiles of CH₃NCO can be discussed by considering two different regions. The first region is defined by radii larger than 200 AU where the temperature is below 50 K. In this region, most of the CH₃NCO in the grains is inherited from the cold

core phase. The second region is defined by radii smaller than 100 AU where the temperature reaches above 100 K and the gas phase abundance of CH₃NCO increases sharply. The CH₃NCO abundance on grains has an inverse profile showing that at low temperature, the CH₃NCO molecules are formed on the grains and are thermally desorbed in the inner part of the envelope.

Martín-Doménech et al. (2017) has determined an upper limit of 1.4×10^{-10} (with respect to molecular H₂) for CH₃NCO in the envelope of IRAS 16293 B at about 60 AU from the central protostar. Another study by Ligterink et al. (2017) has also determined an upper limit of 3.3×10^{-10} (with respect to molecular H₂) for CH₃NCO in the same source IRAS 16293 B. Our model is in agreement with these upper limits at this radius (2×10^{-10}). At 60 AU, the gas phase CH₃NCO/HNCO abundance ratio from our model is 2×10^{-2} which is also reasonably close to the ratio 8×10^{-2} measured by Martín-Doménech et al. (2017) and Ligterink et al. (2017). The ice phase CH₃NCO/HNCO ratio from our model in the outer part of the envelope (> 1000 AU) where possible comets should be formed is of the order of 3.7. This is very close to the CH₃NCO/HNCO ~ 4.33 ratio initially measured by the Philae lander on the comet 67P/Churyumov-Gerasimenko (Goesmann et al. 2015). This observation is, however, now questioned (can only be considered as an upper limit) by the recent measurement from the Double Focusing Mass Spectrometer (DFMS) of the ROSINA experiment (Altwegg et al. 2017).

5 CONCLUSION AND PERSPECTIVES

In this letter, we have provided new insights concerning the chemistry of CH₃NCO in the ISM. Our computation allowed us to confirm the hypothesis made by Cernicharo et al. (2016) about its grain surface origin. Moreover, we tested the impact of these new kinetic data on the prediction of CH₃NCO abundance in the low mass protostar IRAS 16293-2422 and on the CH₃NCO/HNCO abundance ratio observed by the Philae lander on the comet 67P/Churyumov-Gerasimenko. However, the study of the CH₃NCO/HNCO abundance ratio in high mass protostars with proper chemodynamical model is out of the scope of the current letter, but could be done in the near future by comparing with the observations in SgrB2 (N) (Halfen et al. (2015); Belloche et al. (2017)) and in Orion KL (Cernicharo et al. 2016).

ACKNOWLEDGEMENTS

LM, PG, VW and AC thanks ERC starting grant (3DICE, grant agreement 336474) for funding during this work. LM also acknowledges partial support from the NASA postdoctoral program. VW, PG and JCL acknowledge the French program Physique et Chimie du Milieu Interstellair (PCMI) funded by the Conseil National de la Recherche Scientifique (CNRS) and Centre National d'Etudes Spatiales (CNES). A portion of this research was carried out at the Jet Propulsion Laboratory, California Institute of Technology, under a contract with the National Aeronautics and Space Administration.

REFERENCES

- Agúndez M., Wakelam V., 2013, *Chemical Reviews*, **113**, 8710
 Altwegg K., et al., 2016, *Science Advances*, **2**, e1600285
 Altwegg K., et al., 2017, *MNRAS*, **469**, S130
 Anicich V. G., 1993, *Journal of Physical and Chemical Reference Data*, **22**, 1469
 Belloche A., et al., 2017, *A&A*, **601**, A49
 Biver N., et al., 2014, *A&A*, **566**, L5
 Biver N., et al., 2015, *Science Advances*, **1**, e1500863
 Cernicharo J., Kahane C., Guelin M., Gomez-Gonzalez J., 1988, *A&A*, **189**, L1
 Cernicharo J., et al., 2016, *A&A*, **587**, L4
 Crovisier J., 2006, in Daniela L., Sylvio Ferraz M., Angel F. J., eds, *IAU Symposium Vol. 229, Asteroids, Comets, Meteors*. pp 133–152, doi:10.1017/S174392130500671X
 Crovisier J., Bockelée-Morvan D., Colom P., Biver N., Despois D., Lis D. C., Teamtargat-of-opportunity radio observations of comets 2004, *A&A*, **418**, 1141
 Garrod R. T., Wakelam V., Herbst E., 2007, *A&A*, **467**, 1103
 Goesmann F., et al., 2015, *Science*, **349**
 Gratier P., Pety J., Guzmán V., Gerin M., Goicoechea J. R., Roueff E., Faure A., 2013, *A&A*, **557**, A101
 Halfen D. T., Ilyushin V. V., Ziurys L. M., 2015, *ApJ*, **812**, L5
 Hartogh P., et al., 2011, *Nature*, **478**, 218
 Hasegawa T. I., Herbst E., 1993, *MNRAS*, **261**, 83
 Hincelin U., Wakelam V., Hersant F., Guilloteau S., Loison J. C., Honvault P., Troe J., 2011, *A&A*, **530**, A61
 Jiang B., Guo H., 2013, *J. Chem. Phys.*, **139**, 224310
 Kahane C., Ceccarelli C., Faure A., Caux E., 2013, *ApJ*, **763**, L38
 Kammrath A., Verlet J. R. R., Griffin G. B., Neumark D. M., 2006, *J. Chem. Phys.*, **125**, 076101
 Ligterink N. F. W., et al., 2017, *MNRAS*, **469**, 2219
 Majumdar L., Gratier P., Vidal T., Wakelam V., Loison J.-C., Hickson K. M., Caux E., 2016, *MNRAS*, **458**, 1859
 Martín-Doménech R., Rivilla V. M., Jiménez-Serra I., Quénard D., Testi L., Martín-Pintado J., 2017, *MNRAS*, **469**, 2230
 Masunaga H., Inutsuka S.-i., 2000, *ApJ*, **531**, 350
 Mumma M. J., Charnley S. B., 2011, *ARA&A*, **49**, 471
 Neufeld D. A., Wolfire M. G., Schilke P., 2005, *ApJ*, **628**, 260
 Pascal R., Boiteau L., Commeyras A., 2005, *From the Prebiotic Synthesis of α -Amino Acids Towards a Primitive Translation Apparatus for the Synthesis of Peptides*. Springer Berlin Heidelberg, Berlin, Heidelberg, pp 69–122, doi:10.1007/b136707, http://dx.doi.org/10.1007/b136707
 Ruaud M., Loison J. C., Hickson K. M., Gratier P., Hersant F., Wakelam V., 2015, *MNRAS*, **447**, 4004
 Ruaud M., Wakelam V., Hersant F., 2016, *MNRAS*, **459**, 3756
 Rubin R. H., Swenson Jr. G. W., Benson R. C., Tigelaar H. L., Flygare W. H., 1971, *ApJ*, **169**, L39
 Sumathi R., Nguyen M. T., 1998, *The Journal of Physical Chemistry A*, **102**, 8013
 Wakelam V., Vastel C., Aikawa Y., Coutens A., Bottinelli S., Caux E., 2014, *MNRAS*, **445**, 2854
 Wakelam V., et al., 2015a, *ApJS*, **217**, 20
 Wakelam V., Loison J.-C., Hickson K. M., Ruaud M., 2015b, *MNRAS*, **453**, L48
 Wakelam V., Loison J.-C., Mereau R., Ruaud M., 2017, preprint, (arXiv:1701.06492)
 Wight C. A., Beauchamp J. L., 1980, *The Journal of Physical Chemistry*, **84**, 2503
 Zhao Y., Truhlar D. G., 2008, *Theoretical Chemistry Accounts*, **120**, 215
 de Koning M., Fazzio A., da Silva A. J. R., Antonelli A., 2016, *Physical Chemistry Chemical Physics (Incorporating Faraday Transactions)*, **18**, 4652
 van Broekhuizen F. A., Pontoppidan K. M., Fraser H. J., van Dishoeck E. F., 2005, *A&A*, **441**, 249

Appendix:

A large part of the reactions treated in this study have unknown reaction rates (without experimental measurements and/or theoretical calculations to rely upon) in the temperature range of interest (T in the 10-50 K range) but also unknown exothermicity. To make a reasonable estimate of their reaction rates at low temperature, we performed quantum chemical calculations. For our calculations, we have used DFT method using the M06-2X functional with the cc-pVTZ basis set. This highly nonlocal functional developed by Zhao and Truhlar 2008 is well suited for structures and energetics of the transition states.

Table 1: Relative energies at the M06-2X/aug-cc-pVTZ level (in kJ/mol at 0 K including ZPE) with respect to the HCN + CO energy, geometries and frequencies (in cm^{-1} , unscaled) of the various stationary points. The absolute energies at the M06-2X/aug-cc-pVTZ level including ZPE in hartree are also given in column 1.

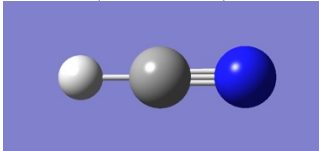
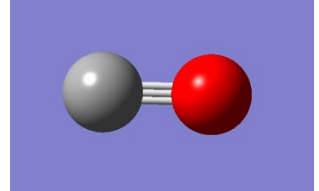
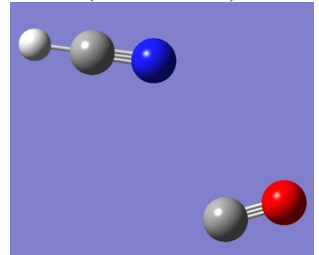
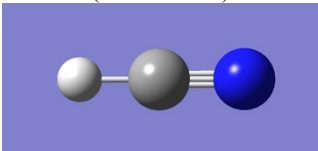
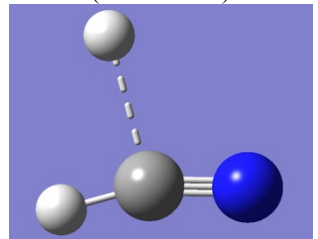
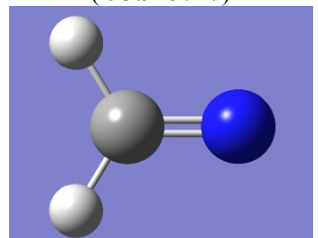
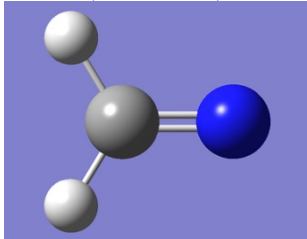
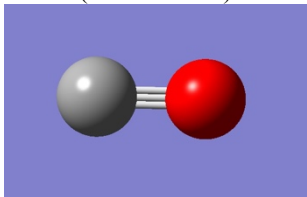
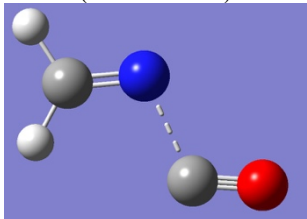
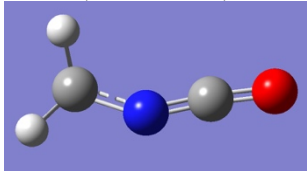
Species (Energy, hartree)	Relative energies (kJ/mol)	Geometries (Position of the atoms in Cartesian coordinates)			Harmonic Frequencies (cm^{-1})	
		x	y	z		
HCN (-93.407418) 	0	C	0.000000	0.000000	-0.494880	789, 789, 2248, 3448
		H	0.000000	0.000000	-1.560893	
		N	0.000000	0.000000	0.647167	
CO (-113.315083) 		C	0.000000	0.000000	-0.640800	2260
		O	0.000000	0.000000	0.480600	
HCN...CO (-206.722951) 	-1.2	C	-2.315172	0.203401	0.000202	22, 61, 67, 78, 791, 804, 2254, 2261, 3453
		H	-3.165133	0.847465	0.000675	
		N	-1.404659	-0.485993	-0.000321	
		O	2.154516	-0.324565	0.000274	
		C	1.608775	0.655100	-0.000305	

Table 2: Relative energies at the M06-2X/aug-cc-pVTZ level (in kJ/mol at 0 K including ZPE) with respect to the H + HCN energy, geometries and frequencies (in cm^{-1} , unscaled) of the various stationary points. The absolute energies at the M06-2X/aug-cc-pVTZ level including ZPE in hartree are also given in column 1.

Species (Energy, hartree)	Relative energies (kJ/mol)	Geometries (Position of the atoms in Cartesian coordinates)	Harmonic Frequencies (cm^{-1})
H (-0.4982065)	0	x y z	
HCN (-93.407418) 		C 0.000000 0.000000 -0.494880 H 0.000000 0.000000 -1.560893 N 0.000000 0.000000 0.647167	789, 789, 2248, 3448
TS (-93.894842) 		N 0.097054 -0.717467 0.000000 C 0.097054 0.436285 0.000000 H 0.394533 1.463794 0.000000 H -1.656237 0.940767 0.000000	505, 779, 921, 2134, 3388, 889i*
H ₂ CN (-93.945717) 	-105.3	C 0.000000 0.000000 -0.501313 N 0.000000 0.000000 0.735111 H 0.000000 0.937025 -1.068947 H 0.000000 -0.937025 -1.068947	948, 1012, 1384, 1749, 3005, 3072

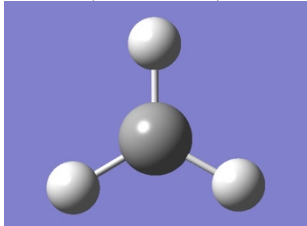
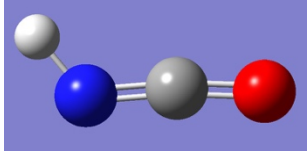
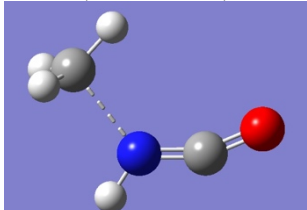
*: imaginary frequency

Table 3: Relative energies at the M06-2X/aug-cc-pVTZ level (in kJ/mol at 0 K including ZPE) with respect to the H₂CN + CO energy, geometries and frequencies (in cm⁻¹, unscaled) of the various stationary points. The absolute energies at the M06-2X/aug-cc-pVTZ level including ZPE in hartree are also given in column 1.

Species (Energy, hartree)	Relative energies (kJ/mol)	Geometries (Position of the atoms in Cartesian coordinates)			Harmonic Frequencies (cm ⁻¹)
		x	y	z	
H ₂ CN (-93.945717) 	0	C 0.000000	0.000000	-0.501313	948, 1012, 1384, 1749, 3005, 3072
		N 0.000000	0.000000	0.735111	
		H 0.000000	0.937025	-1.068947	
		H 0.000000	-0.937025	-1.068947	
CO (-113.315083) 		C 0.000000	0.000000	-0.640800	2260
		O 0.000000	0.000000	0.480600	
TS (-207.244021) 	44.1	C 1.719507	0.198906	0.000021	99, 294, 442, 5459, 1062, 1082, 1415, 1722, 461i*
		H 2.715274	-0.248015	0.000178	
		H 1.639585	1.285638	-0.000032	
		N 0.731882	-0.567158	-0.000051	
		O -1.840088	-0.111857	0.000040	
		C -0.845729	0.438984	-0.000040	
CH ₂ NCO (-207.290007) 	-76.7	C -1.778814	0.139360	0.000083	134, 261, 417, 544, 629, 974, 1133, 1490, 1557, 2410, 3175, 3309
		H -1.993176	1.195587	-0.000180	
		H -2.555836	-0.603926	0.000319	
		N -0.496439	-0.287279	-0.000136	
		C 0.672696	-0.037344	-0.000042	
		O 1.832599	0.100900	0.000071	

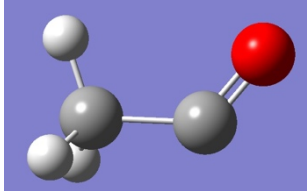
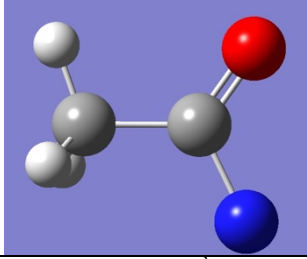
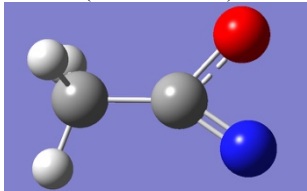
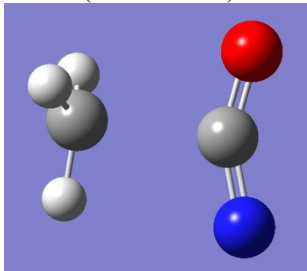
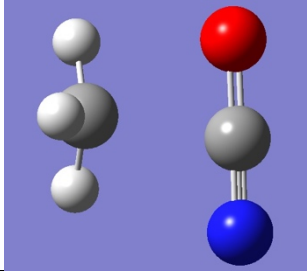
*: imaginary frequency

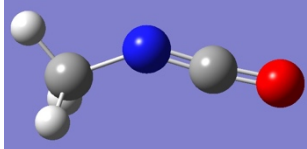
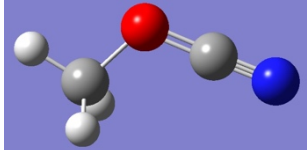
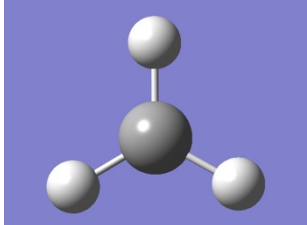
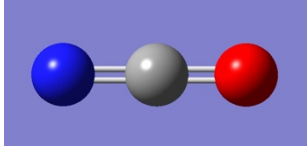
Table 4: Relative energies at the M06-2X/aug-cc-pVTZ level (in kJ/mol at 0 K including ZPE) with respect to the CH₃ + HNC energy, geometries and frequencies (in cm⁻¹, unscaled) of the various stationary points. The absolute energies at the M06-2X/aug-cc-pVTZ level including ZPE in hartree are also given in column 1.

Species (Energy, hartree)	Relative energies (kJ/mol)	Geometries (Position of the atoms in Cartesian coordinates)			Harmonic Frequencies (cm ⁻¹)	
		x	y	z		
CH ₃ (-39.795501) 	0	C	0.000000	0.000000	0.000000	524, 1416, 1416, 3133, 3310, 3310
H		0.000000	1.076523	0.000000	0.000000	
HNC (-168.665769) 		N	1.154466	-0.122413	0.000026	567, 660, 787, 1371, 2369, 3698
C	-0.045063	0.016768	-0.000079	-0.000079		
O	-1.204109	0.015868	0.000031	0.000031		
H	1.821983	0.629339	0.000041	0.000041		
TS (-208.429659) 	83.0	C	-0.920547	0.289264	0.000721	101, 159, 252, 551, 591, 669, 674, 969, 1003, 1241, 1432, 1441, 2197, 3109, 3262, 3277, 3704, 747i*
O	-1.786482	-0.500823	-0.000027	-0.000027		
N	0.248291	0.696949	-0.001215	-0.001215		
H	0.499206	1.668765	0.005455	0.005455		
C	1.895977	-0.433809	0.000426	0.000426		
H	1.460329	-1.413255	-0.130380	-0.130380		
H	2.432240	-0.036324	-0.848907	-0.848907		
H	2.309463	-0.223972	0.975670	0.975670		

*: imaginary frequency

Table 5: Relative energies at the M06-2X/aug-cc-pVTZ level (in kJ/mol at 0 K including ZPE) with respect to the N + CH₃CO energy, geometries and frequencies (in cm⁻¹, unscaled) of the various stationary points. The absolute energies at the M06-2X/aug-cc-pVTZ level including ZPE in hartree are also given in column 1.

Species (Energy, hartree)	Relative energies (kJ/mol)	Geometries (Position of the atoms in Cartesian coordinates)			Harmonic Frequencies (cm ⁻¹)
		x	y	z	
N(⁴ S) (-54.58746)	0				
CH ₃ CO(² A') (-153.127903) 		C -0.388178	0.005985	0.047915	62, 469, 867, 958, 1051, 1355, 1460, 1460, 1989, 3050, 3149, 3151
		O 0.332527	-0.003169	0.973347	
		C -0.032493	0.000250	-1.417739	
		H -0.490106	-0.873754	-1.877220	
		H -0.470486	0.882909	-1.879688	
		H 1.049276	-0.012223	-1.552598	
CH ₃ C(N)O(³ A) (-207.821775) 	-279	O -0.867949	-1.010897	-0.000001	85, 380, 518, 522, 844, 942, 1023, 1234, 1389, 1467, 1470, 1692, 3063, 3132, 3176
		C 1.345357	-0.042331	-0.000012	
		H 1.717670	0.484667	-0.878557	
		H 1.717617	0.482425	0.879906	
		H 1.696968	-1.069688	-0.001305	
		C -0.156245	-0.028182	0.000018	
		N -0.760476	1.230407	-0.000010	
CH ₃ C(N)O(¹ A) (-207.815884) 	-264	O -0.961115	-0.798213	-0.000009	141, 361, 434, 544, 913, 981, 1056, 1255, 1404, 1466, 1478, 1944, 3076, 3154, 3173
		C 1.473599	-0.015759	-0.000021	
		H 1.777168	-0.577365	-0.882612	
		H 1.934804	0.967298	-0.000847	
		H 1.777450	-0.575912	0.883383	
		C 0.013128	0.099415	0.000068	
		N -0.960123	0.867106	-0.000020	
TS(³ A) (→ CH ₃ + NCO) (-207.774031) 	-154	O -0.651718	-1.175499	0.000121	127, 265, 443, 509, 653, 673, 992, 1252, 1412, 1432, 1814, 3105, 3263, 3293, 503i*
		C 1.572500	0.110376	0.000428	
		H 1.600004	1.188300	-0.099523	
		H 1.804223	-0.305225	0.969591	
		H 1.844574	-0.474905	-0.865333	
		C -0.503234	0.013874	-0.001984	
		N -0.921522	1.178618	0.000519	
TS(¹ A) (CH ₃ OCN → CH ₃ NCO) (-207.783064) 	-178	O -0.285154	1.199652	-0.001644	135, 454, 535, 606, 848, 912, 1218, 1297, 1432, 1468, 2092, 3151, 3318, 3328, 860i*
		C -1.114689	-0.748877	0.001882	
		H -0.711470	-1.598000	-0.526160	
		H -1.174977	-0.822782	1.076861	
		H -1.875839	-0.171890	-0.495240	
		C 0.555497	0.280798	-0.009050	
		N 1.342667	-0.599438	0.000101	
CH ₃ NCO(¹ A) (-207.933895)	-574				56, 151, 622, 659, 895, 1132, 1160, 1459, 1498,

			1517, 1552, 2415, 3061, 3129, 3154
$\text{CH}_3\text{OCN}({}^1\text{A})$ (-207.891329) 	-462	C 1.480716 0.349286 0.000000 H -2.401061 -0.222819 -0.000183 H -1.408142 0.963121 0.894860 H -1.407932 0.963363 -0.894678 C 0.767246 -0.133253 0.000001 N 1.835008 0.294098 0.000000 O -0.418388 -0.632318 0.000000	154, 235, 551, 644, 938, 1170, 1178, 1252, 1479, 1503, 1503, 2420, 3081, 3166, 3203
CH_3 (-39.795501) 	-188	C 0.000000 0.000000 0.000000 H 0.000000 1.076523 0.000000 H 0.932296 -0.538261 0.000000 H -0.932296 -0.538261 0.000000	524, 1416, 1416, 3133, 3310, 3310
NCO (-167.991408) 		N 0.000000 0.000000 -1.259704 C 0.000000 0.000000 -0.037349 O 0.000000 0.000000 1.130252	545, 619, 1330, 2053

*: imaginary frequency